Development 140, 3541-3551 (2013) doi:10.1242/dev.095760
© 2013. Published by The Company of Biologists Ltd

Cell fate respecification and cell division orientation drive intercalary regeneration in *Drosophila* wing discs

Ada Repiso*,‡, Cora Bergantiños*,§ and Florenci Serras¶

SUMMARY

To understand the cellular parameters that govern *Drosophila* wing disc regeneration, we genetically eliminated specific stripes of the wing disc along the proximodistal axis and used vein and intervein markers to trace tissue regeneration. We found that veins could regenerate interveins and vice versa, indicating respecification of cell fates. Moreover, respecification occurred in cells close to the wound. The newly generated domains were intercalated to fill in the missing parts. This intercalation was driven by increased proliferation, accompanied by changes in the orientation of the cell divisions. This reorientation depended on Fat (Ft) and Crumbs (Crb), which acted, at least partly, to control the activity of the effector of the Hippo pathway, Yorkie (Yki). Increased Yki, which promotes proliferation, affected the final shape and size. Heterozygous *ft* or *crb*, which normally elicit size and shape defects in regenerated wings, could be rescued by *yki* heterozygosity. Thus, Ft and Crb act as sensors to drive cell orientation during intercalary regeneration and control Yki levels to ensure a proper balance between proliferation and cell reorientation. We propose a model based on intercalation of missing cell identities, in which a coordinated balance between orientation and proliferation is required for normal organ shape and size.

KEY WORDS: Imaginal discs, Regeneration, Growth

INTRODUCTION

There are many examples of tissue regeneration in the animal kingdom, ranging from restoration of entire body parts to regeneration of a few tissues. Some organisms, such as planarians, can regenerate from stem cells, but others, such as amphibians, regenerate their limbs from dedifferentiated cells or from precursors of particular cell types (Tanaka and Reddien, 2011). Regeneration in the absence of stem cells requires cell plasticity and, in some cases, the ability to switch between genetic programs. To understand regeneration, it is important to uncover the origin and behavior of regenerating cells, as well as identify changes in genetic programs that control cell fate switches.

Genetic approaches to study regeneration are difficult to implement in many of the classical model organisms. Therefore, sophisticated genetic tools in the assessment of *Drosophila* imaginal discs provide a useful alternative for regeneration studies. Imaginal discs consist of larval epithelial tissues that correspond to the anlage of different adult structures. Early works on imaginal disc regeneration showed that after pieces of a wing or leg imaginal disc were removed by microsurgery, the remaining tissue could regenerate the missing structures (Bryant, 1971; Hadorn and Buck, 1962; Schubiger, 1971). Moreover, extreme cell plasticity during disc transdetermination has been observed (McClure and Schubiger, 2007). Thus, imaginal discs are a suitable tissue for studying cell plasticity driven by cell fate respecification.

Departament de Genètica, Facultat de Biologia, Institut de Biomedicina (IBUB), Universitat de Barcelona, Diagonal 643, Barcelona 08028, Spain.

*These authors contributed equally to this work
‡Present address: Molecular Biology Institute of Barcelona (IBMB) CSIC, Barcelona 08028, Spain
§Present address: Department of Genetics and Development, College of Physicians and Surgeons, Columbia University, 701 West 168th Street, New York, NY 10032, USA
¶Author for correspondence (fserras@ub.edu)

Accepted 25 June 2013

Despite the clear advantages of using *Drosophila* in cell-plasticity studies, the cellular mechanisms driving the recovery of normal organ size and shape are still poorly understood. Two different scenarios can be predicted for disc regeneration. The first considers that regeneration involves a general remodeling of the tissue, recapitulating a more juvenile stage. Normal size and shape can be achieved by scaling the morphogen gradients and assigning new values to the disc cells. The second scenario predicts that regeneration can be achieved by intercalation of the missing positional values without the need for re-scaling the whole disc. Intercalary regeneration has been documented in many organisms (Agata et al., 2003; Iten and Bryant, 1976; Saló and Baguñà, 1985; Stocum, 1975). In insect legs, the graft of a distal fragment onto an amputated host limb results in the intercalation of central structures to complete regeneration (Bohn, 1970; Nakamura et al., 2007). Similarly, combination of wing disc fragments from the dorsalmost zone with the ventralmost fragments induces regeneration of the structures in between (Haynie and Bryant, 1976).

The use of the Gal4/UAS system controlled by the temperature-sensitive Gal80, which inhibits Gal4, enables the direct examination of regeneration through the induction of cell death in specific domains (Bergantiños et al., 2010; Smith-Bolton et al., 2009). To discriminate between general remodeling and intercalation, we used markers of vein and intervein fates to monitor regeneration of wing disc after cell death. The wing primordium is subdivided into veins (L2, L3, L4 and L5) and interveins (A, B C, D and E) (Fig. 1A), which can be scored very easily for fate respecification. Decapentaplegic (Dpp) (the fly BMP2/4-like homolog) and Hedgehog (Hh) (the fly Sonic hedgehog homolog) are the main morphogens patterning the wing along the anteroposterior axis (Schwank and Basler, 2010). Hh emanates from the posterior compartment and is responsible for Dpp expression in the anterior cells along the anteroposterior boundary (Basler and Struhl, 1994; Capdevila et al., 1994; Tabata et al., 1992; Tabata and Kornberg, 1994). At larval stages, Hh, Dpp and their targets organize the wing disc into stripes of cells that alternate between veins and interveins

(Blair, 2007). It has been proposed that once veins have been positioned through the action of gradients, vein restriction borders, rather than morphogens, act as positional references to control cell proliferation and, ultimately, wing size (Díaz-Benjumea and García-Bellido, 1990; García-Bellido and García-Bellido, 1998; Resino et al., 2002).

In this study, we focused on three topics. First, we wondered if we could establish a late stage in larvae where the effect of the Dpp morphogen gradient was minimized, therefore enabling the determination of whether discs could regenerate in conditions that differed from those in development. Second, we explored whether there was local respecification of fates. Third, we investigated the mechanism driving intercalation. We found that in the late stages of development, cells were respecified locally and cell divisions oriented toward the ablated tissue, driving intercalation.

These findings raise the question of how cells can change orientation during regeneration. Intercalary growth indicates that differences in positional values drive regeneration (Satoh et al., 2010). It has been proposed that cells compare the positional values of their neighbors and undergo division when differences exist (García-Bellido, 2009). Therefore, cell-to-cell contacts should be crucial for sensing tissue loss. Planar cell polarity (PCP) genes are required to reorient mitosis in response to cell death (Li et al., 2009). The typical mitotic orientation toward the dorsoventral (DV) boundary found in normally growing discs is randomized in mutants of the PCP protocadherin genes *fat* (*ft*) and *dachsous* (*ds*) (Baena-López et al., 2005; Bryant et al., 1988; Garoia et al., 2005; Li et al., 2009). Thus, the Ft-Ds system is an obvious candidate for driving cell orientation during intercalary regeneration, acting upstream of the Hippo pathway. The latter is a key regulator of tissue growth that has been implicated in regulating regenerative growth in wing imaginal discs (Grusche et al., 2011).

Another candidate is *crumbs* (*crb*), which is a key factor involved in epithelial organization that is integrated in the subapical region of epithelial cells and is a member of a core complex that regulates cell polarity and shape in embryonic epithelia (Bachmann et al., 2001; Tepass et al., 1990). Moreover, Crb forms part of a core complex of proteins linked to the actin cytoskeleton (Médina et al., 2002) and promotes the formation of adherens junctions between neighboring cells (Izaddoost et al., 2002). Crb also acts as a tumor suppressor, transducing extracellular cues to the Hippo pathway to control growth and size (Grzeschik et al., 2010; Ling et al., 2010; Robinson et al., 2010).

The transcriptional coactivator Yorki (Yki), which is the downstream effector of the Hippo pathway, accumulates in the nucleus of regenerating discs (Grusche et al., 2011; Sun and Irvine, 2011). In this study, we showed that reorientation of mitoses during regeneration required Ft and the transmembrane protein Crb, which regulated the orientation of cell divisions and Yki levels to ensure the correct balance between proliferation and orientation that was required for proper regeneration.

MATERIALS AND METHODS

Cell death induction

Cell death was induced as previously described (Bergantiños et al., 2010). The genotypes used for assessing wing discs were *UAS-rpr; ptc-Gal4; tubGal80^{TS}* or *UAS-rpr; sal-Gal4; tubGal80^{TS}*. The induction time used in this work included the 6 hours of Gal80 perdurance. Developmental times after egg laying (AEL) were converted into 25°C equivalents to facilitate staging (Ashburner et al., 2005). Freshly laid eggs were kept at 17°C to prevent *rpr* expression. Larvae were then shifted to 29°C on the eighth day to activate *rpr* for 16 hours (equivalent to inducing at 94 to 110 hours of development at 25°C) and then back to 17°C to inactivate *rpr* and allow regeneration. In these experiments, larvae could regenerate, although pupariation was delayed by ~24 hours (equivalent to 12 hours at 25°C) in *ptc>rpr* and ~48 hours (equivalent to 24 hours at 25°C) in *sal>rpr* flies. The regeneration time or hours after cell death indicated in this work refers to real hours at 17°C.

For cell-lineage experiments of the L3 vein, we used the *ara^{RF209}* (*ara-lacZ*) strain (Gómez-Skarmeta et al., 1996), and for the intervein lineages, we used the *bs/dsrf-lacZ* strain.

Morphogenetic signal blockade

To modify Dpp or Hh signaling, we used *UAS-tkv**, *UAS-tkv^{DN}* and *UAS-ptc^{A2}*. These alleles were driven by the *nub-Gal4* and *tubGal80^{TS}* constructs to control their expression in the whole wing primordium. Larvae were developed at 17°C, allowing normal morphogenetic signaling. At the onset of pupariation, individuals were transferred back to 17°C to allow proper signaling during metamorphosis. The three genotypes used were: (1) *w; nub-Gal4/+; tubGal80^{TS}/UAS-tkv^{DN}*; (2) *w; nub-Gal4/+; tubGal80^{TS}/UAS-tkv**; and (3) *nub-Gal4/+; tubGal80^{TS}/UAS-ptc$^{\Delta 2}$*. For each *tkv^{DN}*, *tkv** and *ptc$^{\Delta 2}$* experiment, we analyzed at least 200 wings and 20 wing discs.

Immunostaining

Immunostaining was performed using standard protocols. The antibodies used were: rabbit anti-β-galactosidase (1:1000) (ICN Biomedicals), mouse anti-Patched (1:50) (Developmental Studies Hybridoma Bank, DSHB); rat anti-CI (1:5) from R. Holmgren (Harvard University), mouse anti-DSRF (1:500) (Active Motif), rat anti-Araucan (1:200) from S. Campuzano (CBMSO-CSIC, Madrid), guinea pig anti-Knirps (1:200) from J. Reinitz (University of Chicago), and rabbit anti-p-Mad (1:100) from G. Morata (CBMSO-CSIC, Madrid). Fluorescently labeled secondary antibodies were from Invitrogen and Jackson Immunochemicals. TO-PRO3 (1:1000) (Invitrogen) was used to label nuclei. Images were captured using a Leica SPE confocal microscope and processed with ImageJ and Adobe Photoshop 7.0.

Clonal analysis

Twin-spot clonal analysis of non-induced and *ptc>rpr*-induced discs was performed. In Fig. 4, the genotypes used were: *FRT19A/hs-Flp, GFP, FRT19A; ptc-Gal4/+; tubGal80^{TS}/+* for control non-induced discs; and *FRT19A/hs-Flp, GFP, FRT19A; ptc-Gal4/+; tubGal80^{TS} /UAS-rpr* for *ptc>rpr* discs.

The temperature shifts to induce clones were undertaken in parallel for control and *ptc>rpr* discs, and tissues were fixed at the same time. Control and *ptc>rpr* larvae were allowed to grow at 17°C until day 6, when they were heat shocked for 45 minutes at 37°C to induce the expression of the Flp recombinase. Temperature was then shifted to 17°C until day 8, when they were transferred to 29°C for 16 hours to induce *rpr* expression. After death, they were shifted back to 17°C to switch off *rpr* expression and allow regeneration. Wing discs were fixed for 20 to 24 hours at the end of induction (equivalent to 120 hours of development at 25°C plus 10 to 12 hours of delay).

Orientation and the size of the clones were measured on stacks of confocal images using ImageJ. Clones in the DV boundary [that were not labeled by *Drosophila serum response factor* (*DSRF*; *bs* – FlyBase)] were discarded to minimize the effects on clone shapes caused by the compartmental boundary. The sizes of each clone area in pixels were compared using the SPSS software (average comparison test based on Student's *t*-test).

Generation of two cell clones

Two wild-type cell clones were generated by heat shock (37°C for 10 minutes) at 88 or 102 hours of development and fixed at 96 or 110 hours, respectively. The genotype of the flies used was*: yw hsFLP; UAS-GFP; Act>CD2>tubGal4*. The two cell clones were monitored under the Leica SPE confocal microscope and the orientation was manually analyzed.

Mitosis orientation

Rabbit anti-phospho-histone H3 (1:1000) (Upstate-Millipore) and mouse anti-alpha-tubulin (1:200) (Invitrogen) were used for detecting spindle orientation. All the experiments were performed as described above, except

that the flies were transferred from 17°C to 29°C at 196 hours of development (equivalent to 98 hours at 25°C). Cell death was induced by a temperature of 29°C for 11 hours. Dissections were performed in wandering larvae. Images were captured using a Leica SPE confocal microscope and processed with ImageJ and Adobe Photoshop 7.0. Angle orientation was manually measured with respect to the DV boundary. For statistics, we measured mitoses in the same area in all cases: dorsal and ventral zones close to the *ptc* domain, avoiding the DV boundary. The genotype used to evaluate control mitotic orientation (i.e. no cell death or *ptc>rpr* OFF) was: *w; ptc-Gal4:UAS-GFP; tubGal80^{TS}*. The genotypes used for the analysis of control mitosis orientation (no cell death) were: *w; yki^{B5}, ptcGal4/+; tubGal80^{TS}, w; ptcGal4 UAS-GFP/ft$^{G\text{-}rv}$; tubGal80^{TS}, w; ptcGal4 UAS-GFP; crb^{11A22}/tubGal80^{TS}*. The genotypes used for the analysis of mitosis orientation after cell death induction were: *UAS-rpr; ptc-Gal4 UAS-GFP; tubGal80^{TS}, UAS-rpr; yki^{B5}, ptc-Gal4/+; tubGal80^{TS}, UAS-rpr; ptc-Gal4 UAS-GFP/ft$^{G\text{-}rv}$; tubGal80^{TS}, UASrpr; ptc-Gal4 UAS-GFP; crb^{11A22}/tubGal80^{TS}, UAS-rpr; yki^{B5}, ptc-Gal4/+; crb^{11A22}/tubGal80^{TS}, UAS-rpr; yki^{B5}, ptc-Gal4/+ ft$^{G\text{-}rv}$; tubGal80^{TS}, UAS-rpr; ptc-Gal4/UAS-yki^{S168A}; tubGal80^{TS}*.

Adult wing parameters after cell death

Wing area and length/height ratio (L/H) were analyzed to evaluate the final size and shape, respectively, of adult wings. For these experiments, we used the *sal$^{E/Pv}$-Gal4* strain that had a *sal* (*salm* – FlyBase) wing enhancer, which confined expression to the wing and subsequently, wing parameters could be scored (Barrio and de Celis, 2004). Measurements were made using ImageJ. After cell death induction, flies were cultured at 17°C until adulthood. The genotypes used for this analysis were (*sal$^{E/Pv}$>rpr* ON): *UAS-rpr; sal$^{E/Pv}$-Gal4; tubGal80^{TS}, UAS-rpr; yki^{B5}, sal$^{E/Pv}$-Gal4/+; tubGal80^{TS}, UAS-rpr; sal$^{E/Pv}$-Gal4/ft^{GRV}; tubGal80^{TS}, UAS-rpr; sal$^{E/Pv}$Gal4; crb^{11A22}/tubGal80^{TS}, UAS-rpr; yki^{B5}, sal$^{E/Pv}$-Gal4/+; crb^{11A22}/tubGal80^{TS}, UAS-rpr; yki^{B5}, sal$^{E/Pv}$-Gal4/+ ft$^{G\text{-}rv}$; tubGal80^{TS}*.

The controls (*sal$^{E/Pv}$>rpr* OFF) were the same genotypes kept at 17°C.

RESULTS

Pattern regeneration involves cell fate respecification

To study whether regeneration can still occur once cells have already been specified, we first determined if there was a phase in which morphogen gradients stopped operating in wing imaginal discs. We genetically altered Dpp signaling and looked for defects in wing patterning. We used two Gal4-inducible alleles of the Dpp type I receptor, *thickveins* (*tkv*) *UAS-tkv**, a constitutively active form (Lecuit and Cohen, 1997), and *UAS-tkv^{DN}*, a kinase-defective form that acts as a dominant-negative allele (Haerry et al., 1998). We ectopically expressed one or the other using *nub-Gal4*, which drives expression in the whole wing primordium. Using this driver, we could analyze alterations in the vein-intervein pattern in the wing disc as well as in adult wings. Using the temperature-sensitive *Gal80^{ts}* construct, which inhibits Gal4 activity (Zeidler et al., 2004), we examined the expression of the transgenes at two different time points: before veins were fully established (78 hours AEL); and after veins were established (105 hours AEL) (Fig. 1; supplementary material Fig. S1). In *nub>tkv^{DN}*-activated discs at 78 hours, the pMad gradient was absent and the adults displayed smaller wings. In these discs, the intervein transcription factor DSRF (Montagne et al., 1996) was uniformly distributed throughout the wing pouch, except for L3 and L5 (supplementary material Fig. S1). When *nub>tkv^{DN}* was activated at 105 hours, the pMad gradient was eliminated, but a nearly normal wing, with all vein and intervein domains, still developed (Fig. 1B,C), demonstrating a temporal requirement for Dpp.

High levels of Dpp signaling in discs after *nub>tkv** activation at 78 hours also resulted in a massive intervein-to-vein transformation (supplementary material Fig. S1D). By contrast, *nub>tkv** activation at 105 hours resulted in a wing that, albeit deformed,

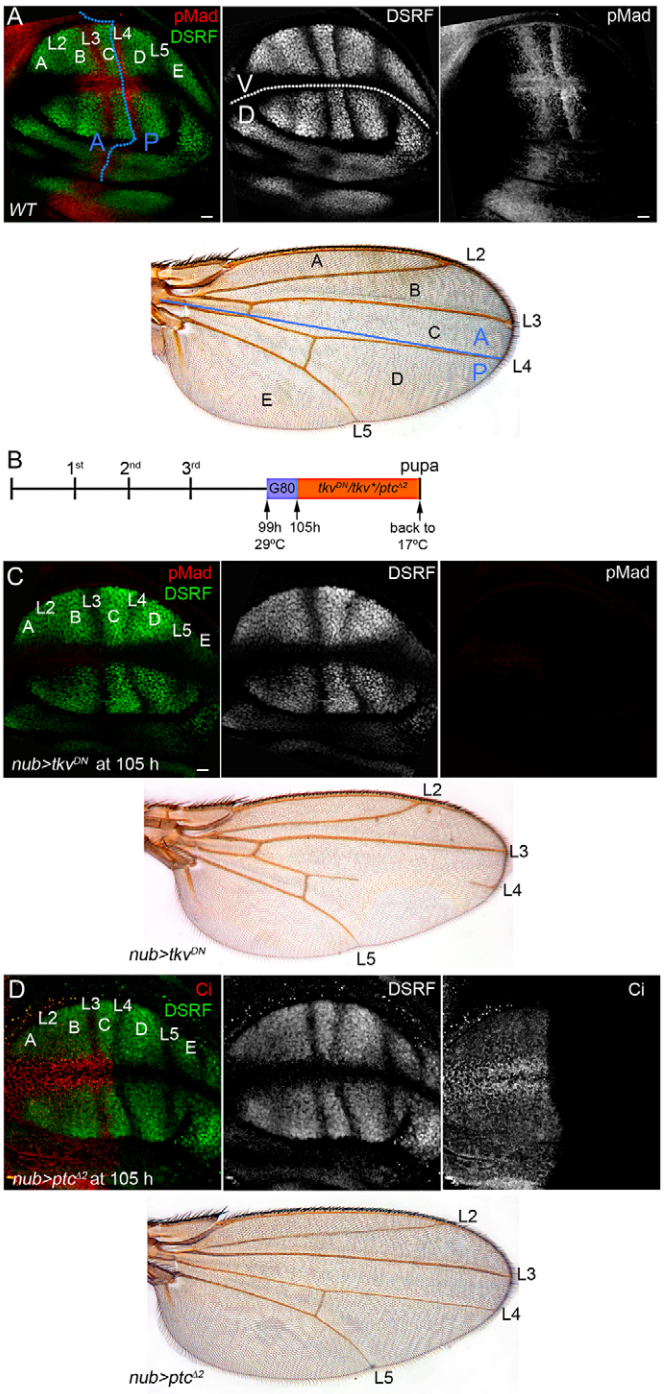

Fig. 1. Dpp and Hh gradients are not involved with vein and intervein positioning in late wing discs. (**A**) Wild-type disc and adult wing. Blue lines: AP boundary. White dotted line: DV boundary. (**B**) Temperature changes performed to activate transgene expression over time (first, second and third larval instars; pupa: onset of pupariation). Larvae were allowed to grow at 17°C (black horizontal line) until 99 hours AEL, when the larvae were shifted to 29°C to activate the transgene. Blue bar: Gal80^{ts} perdurance. Red bar: full transgene expression (from 105 hours onwards). (**C**) Removal of Dpp signaling at 105 hours (shifted at 99 hours; full transgene expression at 105 hours) in *nub>tkv^{DN}* disc and wing. Stripes lacking DSRF: veins. (**D**) Inhibition of Hh signaling at 105 hours of development in *nub>ptc$^{\Delta 2}$* disc and wing. Ci marks A-compartment. Scale bars: 15 µm. WT, wild type.

showed distinguishable vein and intervein regions, with only intervein E being apparently transformed into vein tissue (supplementary material Fig. S1E).

We next tested Hh requirement in the late stages using an allele of the Hh receptor *patched* (*ptc*), *UAS-ptc*^{A2} (Casali, 2010), which is insensitive to Hh binding and thus constitutively inhibits the pathway. When Hh was blocked at 78 hours, growth and vein/intervein organization were abolished (supplementary material Fig. S1F). However, when the inhibition was performed at 105 hours, all vein zones were present in most of the wing imaginal discs (Fig. 1D). In 90% of the adults that emerged, fragments of the L2 and/or L4 wing veins were absent. Interestingly, 10% of these adults developed normal wings with the complete set of veins and interveins (Fig. 1D). Together, these results indicated that in late third instar, veins and interveins could be maintained independently of morphogen gradients and that normal wings could develop in the absence of Hh, albeit at a low frequency.

We next explored whether genetic ablation of wing domains at these late stages resulted in regeneration of the normal vein-intervein pattern. We genetically ablated two different stripes of cells using the *Gal4/Gal80*^{ts} system to activate the proapoptotic gene *reaper* (*UAS-rpr*) (Zhou et al., 1997): (1) *patched* (*ptc*)-*Gal4* driver (hereafter termed *ptc>*) (Hinz et al., 1994), used to eliminate intervein C in the anterior compartment; and (2) *Spalt* (*sal*)-*Gal4* (hereafter *sal>*) (Barrio and de Celis, 2004; de Celis and Barrio, 2000), used to kill the tissue between vein L2 and intervein D, thereby affecting part of the anterior and posterior compartments (Fig. 2A,G). The *Gal80*^{ts} transgene allowed conditional activation of *UAS-rpr*, and thus temporal control of cell death.

In *ptc>rpr* discs right after the induction of the *rpr* transgene (110 hours AEL), intervein C was absent (Fig. 2C). The flanking L3 and L4 veins were brought together apically, and the gap left by the dead cells was healed (compare Fig. 2B-D). L3 cells, which normally express the transcription factor *araucan* (*ara*) (Gómez-Skarmeta et al., 1996), concomitantly upregulated the intervein transcription factor *DSRF* (Fig. 2D). In the period from 5 to 15 hours after death induction, both Ara- and DSRF-positive cells segregated and formed a narrow DSRF-expressing stripe that corresponded to the newly regenerated C domain (Fig. 2E). Eventually, 20 hours after induction, L3 and intervein C were completely re-established (Fig. 2F). Remarkably, regions far from the wound, such as L2, did not show any expression changes, as the expression of the L2 transcription factor *knirps* (*kni*) (Lunde et al., 1998) remained constant from the beginning throughout the regeneration process (Fig. 2C). In summary, *ptc>rpr* experiments, which resulted in elimination of a stripe of anterior cells, showed that respecification only affected C-L3 regions and not the flanking posterior L4 nor the remote L2. This suggested that cell fate respecification was local and compartment specific.

In *sal>rpr* discs observed immediately after *rpr* induction, *kni* expression (L2) at the edge of the death domain was strongly reduced (Fig. 2H); however, the L5 domain, which was far from the posterior wound edge, was not affected (Fig. 2G,J). This indicated that L2 underwent respecification, as observed for L3 in *ptc>rpr* discs. About 15-20 hours after cell death, the ablated domains reappeared: the L4 domain (lacking DSRF in the posterior), intervein C (DSRF-positive stripe and flanked posteriorly by L4), and some anterior cells that were DSRF-positive and co-expressed Ara (emergent L3) (Fig. 2K). At this time point, the newly formed stripes were narrower. Intervein C had a width of 4±1 cells, which contrasted with the 8±1 cells making up the wild-type discs. At 25-30 hours after cell death, all vein/interveins had expanded and reached approximately normal sizes (Fig. 2I,L).

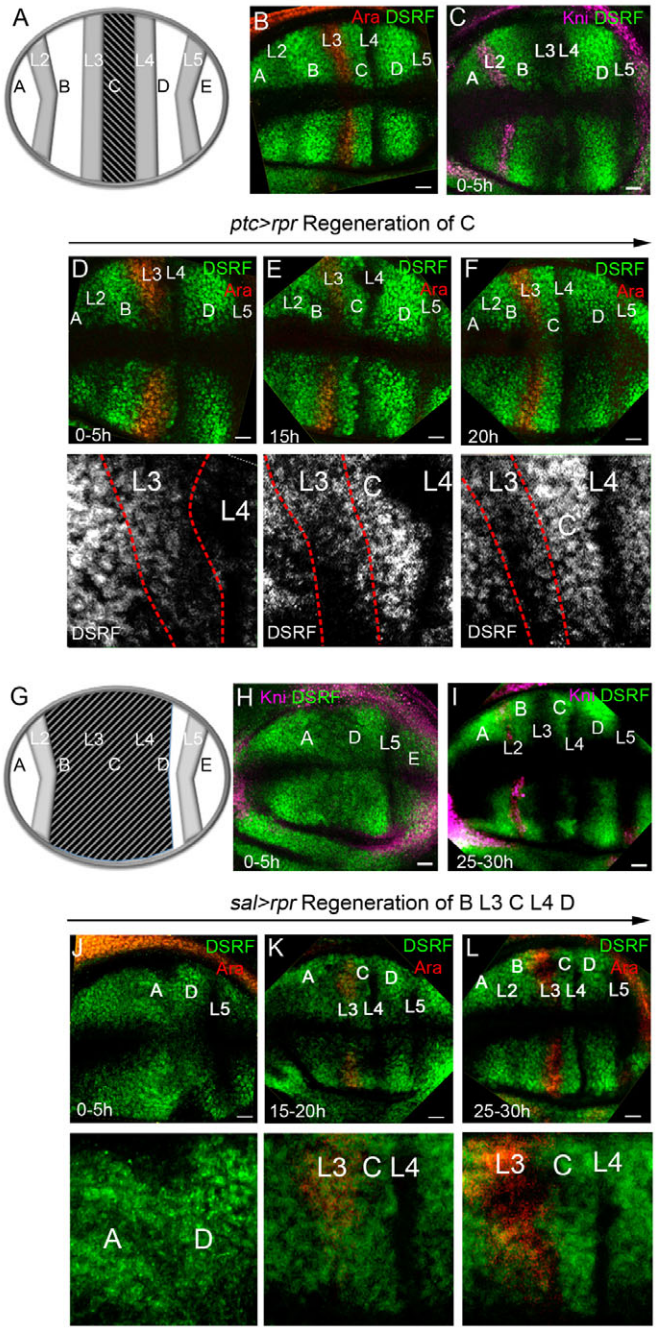

Fig. 2. Regeneration of veins and interveins in *ptc>rpr* and *sal>rpr*. (A,C-F) *ptc>rpr*, (G-L) *sal>rpr*. (**A**) Scheme of the *ptc>rpr* wing disc. (**B**) Wing discs without cell death. (**C**) *ptc>rpr* discs 0 hours after cell death. (**D-F**) *ptc>rpr* discs at different times after *rpr* induction. Top: wing disc area; bottom: high magnifications. Red lines: L3 contour. (**G**) Scheme of the *sal>rpr* wing disc. (**H**,**I**) *sal>rpr* discs 0 hours and 25 hours after cell death. L2 was lost 0 hours after (H) and was not recovered until 25 hours later. (**J-L**) *sal>rpr* discs at different times following *rpr* induction. Top: wing discs; bottom: high magnifications. Scale bars: 15 μm.

Cell lineage supports intercalary growth

As mentioned above, two models can account for the regeneration of the ablated zones. In the first, the whole wing primordium is remodeled by a general shift of veins and interveins and therefore, new cell fates are assigned. According to this model, in *ptc>rpr*

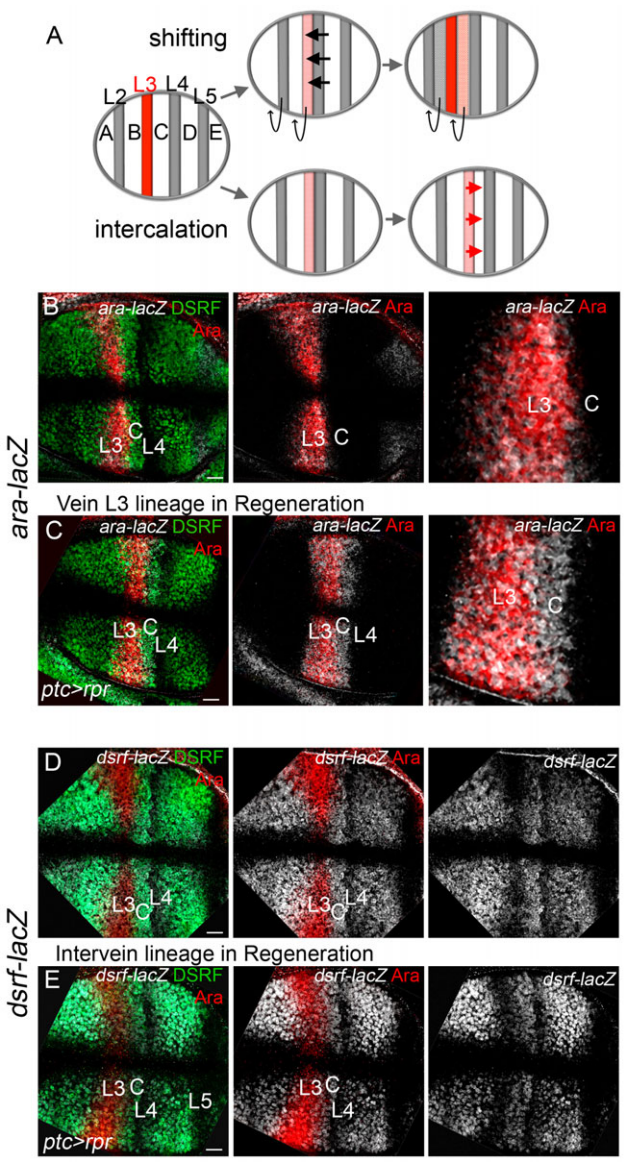

Fig. 3. Cell lineage of the regenerated tissue. (**A**) Models for *ptc>rpr* wing disc regeneration. The L3 in the A-compartment (red) came into contact with the posterior L4. L3 expressed DSRF and Ara concomitantly and transiently (light red). In the shift model, cells of the anterior compartment received the Hh signal (black horizontal arrows) and transformed L3 into C. L3 thus shifted position to the previous B. The Dpp/pMad gradient formed and positioned B at L2, and L2 at E (curved arrows). In the intercalation model, the L3 vein intercalated cells between L3 and L4 to form C, without a general change in the vein and intervein positions. The meeting of the two veins (L3 and L4) resulted in the filling in of the missing intervein C by vein cells belonging to the same compartment in which cell death had occurred (red arrows). (**B**) Non-induced disc carrying the *ara-lacZ* reporter (white) labeled for DSRF (green) and Ara (red). Right: magnification of dorsal L3. (**C**) Induced *ptc>rpr* disc carrying the *ara-lacZ* construct 10 hours after cell death. (**D**) Non-induced disc carrying the *dsrf-lacZ* reporter. (**E**) *ptc>rpr* disc carrying the *dsrf-lacZ* reporter, 15 hours after *rpr* induction. Scale bars: 15 μm.

discs, healing would force L3 (abutting the P compartment) to receive high levels of Hh signaling and intervein B, which normally receives low Hh levels, to now receive intermediate levels (Fig. 3A). This would induce respecification of L3 into intervein C and intervein B into L3. In the second model, respecification only occurs in cells near the dead domain inside the affected compartment. This means that only the L3 vein would change its fate in *ptc>rpr* discs. This L3 would then intercalate newly formed cells between itself and L4 in the P compartment to regenerate intervein C (Fig. 3A). Thus, the second model implies intercalary proliferation and local respecification.

We analyzed the cell lineage of the regenerated zone to examine if global shifting of veins and interveins occurred. We took advantage of the perdurance of two *lacZ* reporter lines, *ara-lacZ* and *dsrf-lacZ* (reporters of Ara and DSRF, respectively), to trace the cell lineages. We have previously demonstrated that when the C domain is ablated, most of the regenerated tissue arises from anterior cells rather than the surviving C (*ptc*) cells (Bergantiños et al., 2010). To investigate the origin of the newly formed C domain, we compared *ara-lacZ* expression with the expression of the Ara protein. We found that *ptc>rpr* discs analyzed 10 hours after cell death expressed high levels of *ara-lacZ*, not only in L3 cells, but also in most of the newly formed intervein C (compare Fig. 3B,C). By contrast, the protein Ara was present only in L3 cells. This demonstrated that the regenerated intervein C arose from the L3 vein.

We also traced the origin of interveins by analyzing the perdurance of the *dsrf-lacZ* reporter and comparing it with the DSRF protein (Fig. 3D). If the action of Hh was to shift positions towards the anterior, as predicted by the first model, e.g. L3 respecified into C and B into L3, high levels of *dsrf-lacZ* (from B) would therefore be found in the new L3. However, if L3 stayed in its original site, as predicted by the second model, L3 cells would show no or only low levels of *dsrf-lacZ*. We found that after *ptc>rpr* induction, *dsrf-lacZ* levels in L3 were absent or much lower than those observed in the intervein regions (Fig. 3E), indicating no shift in positions. In addition, the size of intervein B did not decrease during regeneration (average width from 0 to 5 hours after cell death was of 8±1 cells in both *ptc>rpr* and wild-type discs) and the DSRF protein and *dsrf-lacZ* colocalized in other interveins far from the dead domain (Fig. 3E), demonstrating that interveins maintained their size and identity.

Similarly, during regeneration of *sal>rpr dsrf-lacZ* discs, L4 (defined by the absence of anti-DSRF labeling) and L3 appeared in stripes of *dsrf-lacZ*-positive cells (supplementary material Fig. S2). This indicated that the newly regenerated L3 and L4 had derived from tissue that was previously intervein, reinforcing the idea that vein-intervein fate respecification occurs during wing regeneration. The absence of *dsrf-lacZ* in L5 did not support vein shifting or global remodeling of cell fates. In conclusion, our results supported the second model based on respecification and intercalary growth.

Mitotic orientation drives intercalation

One of the properties that ensures the right size and shape of an organ is the orientation of mitoses. In wing disc development, cells orient divisions along the proximodistal (PD) axis to form the elongated wing with the regular pattern of veins and interveins (García-Bellido and Merriam, 1971; Milán et al., 1996a; Resino et al., 2002). Thus, in the absence of general remodeling of the disc, it is likely that the orientation of growth changes to intercalate cells in order to fill the gap left by the dead cells.

To address whether intercalation was driven by changes in growth orientation, we induced clones and analyzed their shape and orientation in wild-type and regenerating discs. Clone orientation

was measured in relation to the angle between the DV boundary and the longest clone axis. Angles were grouped into three categories: 0-35°, for clones growing parallel to the DV boundary; and 36-55° or 56-90°, for those growing halfway or fully perpendicular to the DV boundary, respectively. In control discs with no cell death, most of the clones oriented perpendicular to the DV boundary (*n*=295; Fig. 4A,A′), in agreement with previous reports (García-Bellido and Merriam, 1971; Milán et al., 1996a; Resino et al., 2002). However, in *ptc>rpr* discs, most of the clones oriented toward the wound (category 0-35°) (*n*=251; Fig. 4B,B′). Thus, cells close to the wound changed their growth orientation in order to fill the ablated region, suggesting the presence of a mechanism that senses a lack of tissue after cell death or injury. Although the most evident changes in orientation were found in the central L3-C zone, some reorientation was also detected in the most anterior compartment, between B and L2, and in the posterior compartment, albeit less frequently.

We also studied possible differences in clone size by measuring areas of clones in different zones. We found that clone areas of *ptc>rpr* discs increased in the L3-C zone, compared with other zones of the disc (average for control, 1258 px, and for *ptc>rpr*, 2526 px) (Fig. 4C). This was consistent with previous observations that cells near the wound increase their rate of division after cell ablation (Bergantiños et al., 2010; Smith-Bolton et al., 2009). By contrast, the most anterior zones that extended between the L2 and B region showed a small increase in clone area (Fig. 4C). We also observed that clone size in the *ptc>rpr* L4-D zone of the posterior compartment was strongly reduced (average for control, 2045 px, and for *ptc>rpr*, 532 px), indicating that the undamaged posterior compartment displayed slow growth while the anterior was regenerating. This non-autonomous reduction of growth may be important for maintaining the tissue proportions and shape (Mesquita et al., 2010).

Next, we tested whether these changes in clone orientation correlated with mitotic orientation. We first monitored mitotic orientation with respect to a virtual DV boundary in the *ptc* domain of normal discs. At 96 hours of development, a large number of mitoses oriented with angles between 55 and 90° with respect to the DV boundary, as described before (Baena-López et al., 2005) (Fig. 5A,B). However, at 110 hours of development, the mitosis angle distribution was more random. Random distribution of mitotic orientation at these stages is followed by preferential allocation of the postmitotic cells along the PD axis (Milán et al., 1996b; Resino et al., 2002). To further test these observations, we generated two cell clones and monitored their orientation at 96 and 110 hours of development, obtaining the same distribution as that for mitotic spindle orientation (supplementary material Fig. S3).

For the study of mitotic orientation in *ptc>rpr* discs, we focused our analysis at 110 hours of development, as endogenous proliferation is lower at this time than at 96 hours. After *ptc>rpr* induction, more that 50% of mitoses belonged to the 0-35° group (Fig. 5C,D), indicating that cell divisions were reoriented toward the dead domain, as found for the clonal analysis.

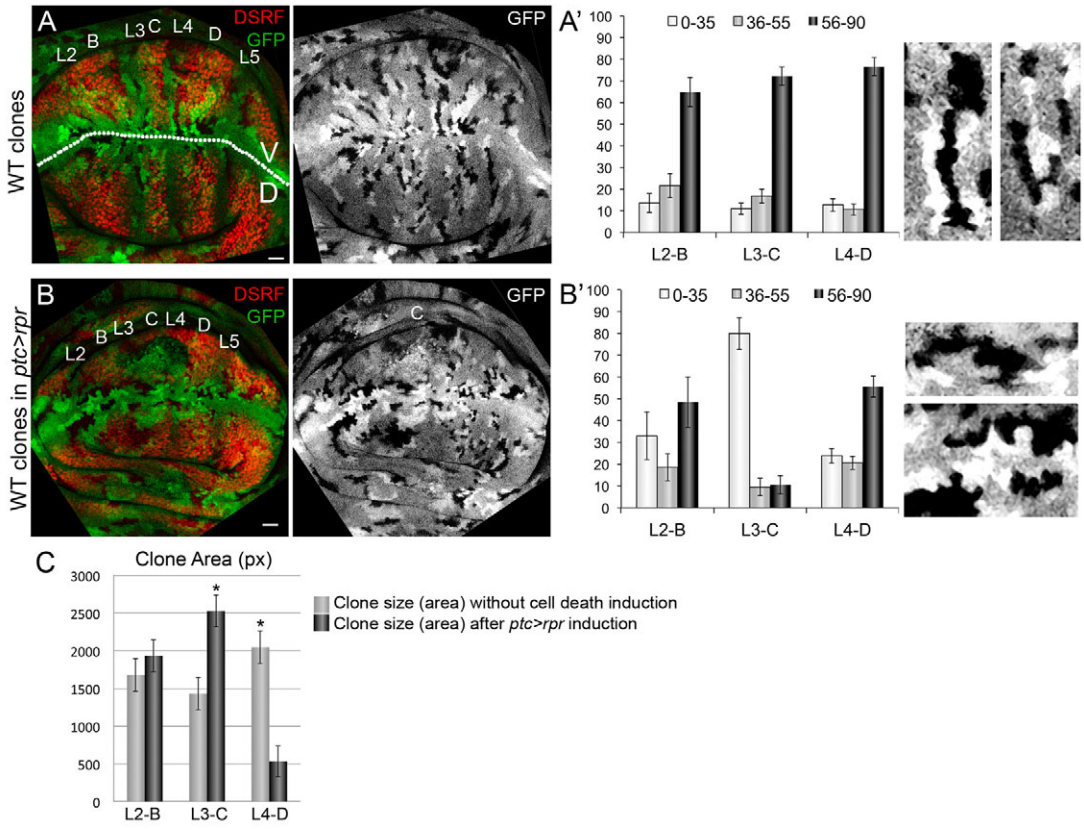

Fig. 4. Orientation of clones during regeneration. (**A**,**A′**) Twin clones marked by GFP (bright green and black) in non-induced wing disc. Dotted line, DV boundary. Gray, GFP channel. (A′) Distribution of clone orientation in non-induced discs. L2-B, L3-C, and L4-D indicate the different zones analyzed. (**B**,**B′**) Twin clones in *ptc>rpr*-induced wing disc. (B′) Distribution of clone orientation of *ptc>rpr* discs. Right: magnification of clones. Scale bars: 15 μm. (**C**) Average area of clones in pixels in non-induced (gray bars; *n*=295) and *ptc>rpr*-induced (black bars; *n*=251) discs. **P*<0.001.

DEVELOPMENT

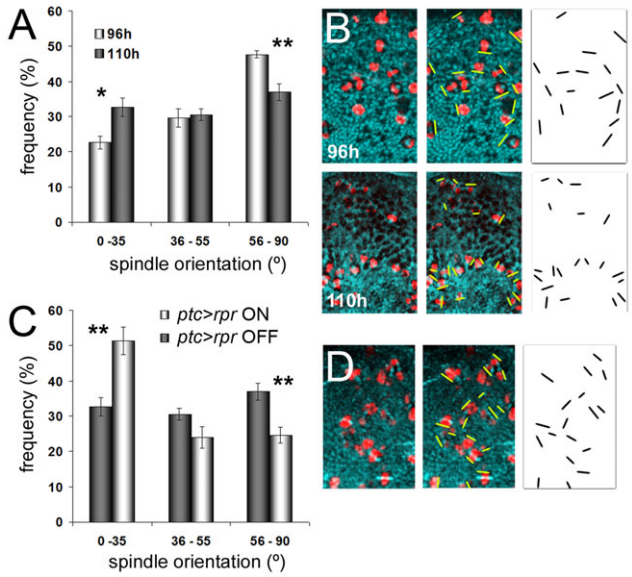

Fig. 5. Mitosis orientation in the *ptc* domain during normal growth and regeneration of the wing disc. (**A**) Angle distribution with respect to the DV boundary in the *ptc* domain of wing discs at 96 hours and 110 hours of normal growth. (**B**) Magnified images of dividing cells at 96 hours (top row) and 110 hours (bottom row). Division orientations were scored by marking with a yellow line on the confocal image (middle) and representing the final scores on a chart (right). (**C**) Angle distribution with respect to the DV boundary in regenerating *ptc>rpr* wing discs. (**D**) Magnified image of dividing cells after *ptc>rpr* induction. **P*<0.01, ***P*<0.001, Student's *t*-test. Phospho-histone H3 (red) and alpha-tubulin (blue) are also shown.

Fat and Crumbs are required for mitosis orientation during tissue regeneration

We next examined whether *ft* was involved in cell division orientation after genetic ablation. We focused our attention on *ft*, which is expressed in the whole wing pouch and antagonizes Dpp during growth regulation (Schwank et al., 2011). We used the null $ft^{G\text{-}rv}$ allele, which is lethal in homozygosis, but results in normal wings in heterozygosis (Bryant et al., 1988; Garoia et al., 2005; Mahoney et al., 1991). Our rationale was that $ft^{G\text{-}rv}$/+ heterozygotes would confer a sensitized background, in which the response required to regenerate would be compromised under stress conditions. We found that *ptc>rpr* $ft^{G\text{-}rv}$/+ discs regenerated, but unlike wild-type backgrounds, failed to reorient mitosis toward the cell death domain. Only 23% of the mitoses fell into the 0-35° group, whereas 45% had an orientation of 56-90° (Fig. 6A).

Failure in reorientation should result in abnormally regenerated adult wing shape. To test this, we used $sal^{E/Pv}$>*rpr*, which acts only in the wing discs and enables the examination of regeneration in $ft^{G\text{-}rv}$/+ adult wings. We found that $ft^{G\text{-}rv}$/+ regenerated wings were more elongated than those of controls (Fig. 6C). This observation agreed with the failure to reorient divisions toward the damaged tissue. In addition, we also found size effects, as the area of regenerated wings was larger compared with control (Fig. 6D).

These observations prompted us to reason that Ft is rate limiting under regenerative conditions and that the final size is uncontrolled in $ft^{G\text{-}rv}$/+ heterozygotes, probably caused by a failure of reorientation and excessive cell proliferation. Yki also accumulates in *ft* mutants (Bennett and Harvey, 2006; Cho et al., 2006; Silva et al., 2006; Tyler and Baker, 2007; Willecke et al., 2006), explaining why amorphic *ft* alleles in homozygosis result in hyperplastic discs and lethality (Bryant et al., 1988; Mahoney et al., 1991).

We decided to test whether an independent cell-to-cell contact mechanism that controls proliferation driven by Yki affected orientation. To this end, we used mutant heterozygous discs for the null crb^{11A22} allele, which elicits a phenotypically wild-type wing in normal conditions. Unlike in wild-type discs, after *ptc>rpr* induction, only 28% of the crb^{11A22}/+ mitoses faced the wound (0-35°) and 42% of the mitoses belonged to the 56-90° class (Fig. 6B). Thus, heterozygous crb^{11A22}/+ failed to reorient mitosis toward the cell death domain. We also used $sal^{E/Pv}$>*rpr* to examine regeneration in crb^{11A22}/+ wings and found that the regenerated wings were more elongated and larger, indicating effects on shape and size (Fig. 6C,D). The phenotypes observed in heterozygosity were specific, as heterozygosity for alleles of unrelated genes (i.e. JNK pathway) has been demonstrated to induce opposite effects, such as regeneration impairment (Bergantiños et al., 2010).

Yki-driven proliferation and mitotic orientation act in a coordinated manner

It is possible that *ft* or *crb* heterozygotes not only have a reduced ability to reorient, but also exhibit excessive proliferation caused by unrestrained Yki activity, which could interfere with reorientation. To test whether *yki* in excess disrupted orientation, we overexpressed *UAS-*yki^{S168A}, which acts as a constitutively active form because it cannot be targeted by the inhibitory phosphorylation of the Warts kinase of the Hippo pathway (Dong et al., 2007). The *UAS-*yki^{S168A} transgene was expressed concomitantly with *UAS-rpr*. However, the 11 hours of *rpr* activation used in this experiment did not completely eliminate the *ptc* domain (Bergantiños et al., 2010). Therefore, it is likely that *UAS-*yki^{S168A} overexpression acts on surviving cells as well as on newly divided cells, contributing to the regenerated *ptc* domain. In these conditions, most of the mitotic orientations belonged to the 55-90° group with respect to the DV axis, the overall distribution being similar to those of the *ft* or *crb* mutant backgrounds shown above (Fig. 6E). Thus, overexpression of *UAS-*yki^{S168A} in *ptc>rpr* discs resulted in failure of reorientation toward the wound. Moreover, adult wings regenerated after *UAS-*yki^{S168A} $sal^{E/Pv}$>*rpr* activation were slightly larger and elongated (Fig. 6G,H).

Thus, we hypothesized that normal organ size and shape require a balance between proliferation and cell reorientation that is controlled by cell-to-cell contacts. In this hypothesis, *ft* or *crb* mutations, by inducing excessive *yki*-driven proliferation, unbalance this equilibrium and perturb the final proportions of the organ. If this is true, the absence of reorientation due to *ft* or *crb* heterozygosity should be rescued by a decrease in *yki* expression. To test this, we generated double heterozygotes for either *ft* or *crb* and one copy of the yki^{B5} loss-of-function allele. Yki^{B5} heterozygous wings were normal in size and shape. However, yki^{B5}/+ heterozygotes under *ptc>rpr* ablation could not reorient mitosis upon cell death induction (Fig. 6F) and elicited less elongated and smaller wings under $sal^{E/Pv}$>*rpr* (Fig. 6G,H). We analyzed the double heterozygous mutant $ft^{G\text{-}rv}$/+ yki^{B5}/+ and found that after *ptc>rpr* induction, 46% of mitoses belonged to the 0-35° class (Fig. 6I), indicating reorientation toward the wound. This was similar to that observed in the wild-type condition, in which 52% of mitoses belonged to the 0-35° class after *ptc>rpr* induction (Fig. 5C). In addition, $ft^{G\text{-}rv}$/+ yki^{B5}/+ in $sal^{E/Pv}$>*rpr* rescued normal wing size and shape (Fig. 6J). We also examined the double heterozygous mutant crb^{11A22}/+ yki^{B5}/+ and found that the effect of

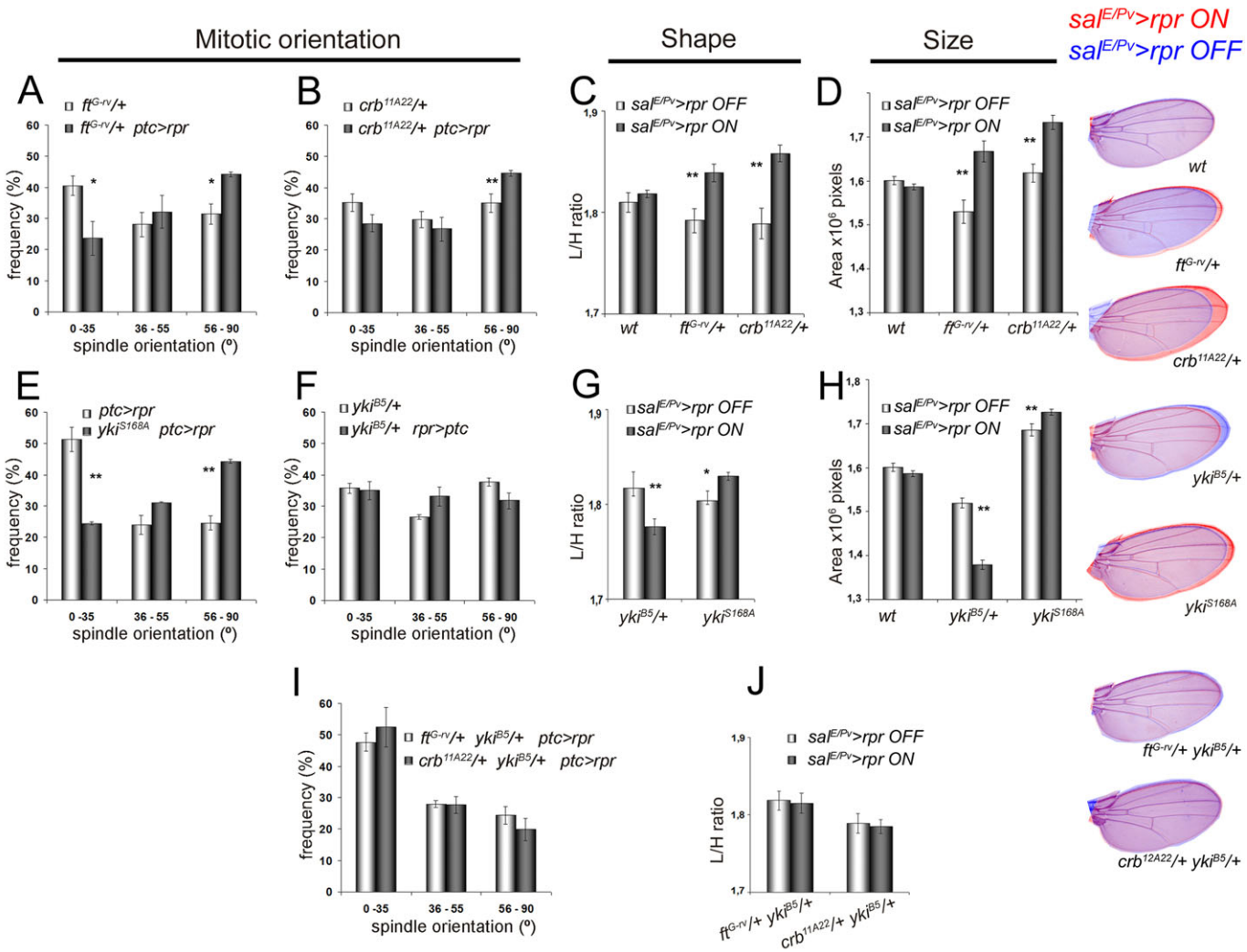

Fig. 6. Mitotic orientation, shape and size in different genetic backgrounds of regenerated wing discs and adult wings. Distribution of mitoses for $ft^{G\text{-}rv}$/+ (**A**), crb^{11A22}/+ (**B**), *UAS-yki*^{S168A} (**E**), yki^{B5}/+ (**F**) and the double heterozygotes $ft^{G\text{-}rv}$/+ yki^{B5}/+ and crb^{11A22}/+ yki^{B5}/+ (**I**). Note that in E, *ptc>rpr* mitoses are plotted with and without the *UAS-yki*^{S168A} transgene. The shape of the adult wings after $sal^{E/Pv}$>*rpr* cell death in different mutants is given as the length/height (L/H) ratio for wild type, $ft^{G\text{-}rv}$/+ and crb^{11A22}/+ (**C**), yki^{B5}/+ and *UAS-yki*^{S168A} (**G**) and $ft^{G\text{-}rv}$/+ yki^{B5}/+ and crb^{11A22}/+ yki^{B5}/+ double mutants (**J**). Areas of adult wings are shown for wild type, $ft^{G\text{-}rv}$/+ and crb^{11A22}/+ (**D**) and wild type, yki^{B5}/+ and *UAS-yki*^{S168A} (**H**). The right column shows examples of adult wings for the indicated genotypes, with the $sal^{E/Pv}$>*rpr* ON (red) and $sal^{E/Pv}$>*rpr* OFF (blue) images superimposed. *P<0.01, **P<0.001, Student's *t*-test.

the *crb* mutation after *ptc>rpr* or $sal^{E/Pv}$>*rpr* induction was also rescued by yki^{B5}/+ heterozygosity (Fig. 6I,J).

DISCUSSION

The results reported here support a model for epithelial regeneration that involves: (1) local respecification of vein and intervein fates; (2) increase in proliferation near the damaged tissue; and (3) reorientation of cell division regulated by cell-to-cell contacts. These properties drive intercalation of new cells between different positional values, for example, when two opposing veins intercalate to form an intervein.

Intercalation has been linked to the regeneration of limbs, appendages and body parts in many organisms (Bryant and Iten, 1977; French, 1976; Haynie and Bryant, 1976; Nakamura et al., 2007). In amphibians, it has been proposed that intercalation results from interactions among cells located near a wound, stimulating proliferation and the restoration of the structures in between (Satoh et al., 2010). In *Drosophila* wing discs, when small fragments of distant zones are cultured separately, they produce mirror-image duplicated structures (Bryant, 1971; Karlsson and Smith, 1981; Kirby et al., 1982; Schubiger, 1971; Schubiger and Alpert, 1975). However, when those fragments are juxtaposed and cultured together, they intercalate to form the structures in between (Haynie and Bryant, 1976).

With our experimental approach, we could re-evaluate the process of intercalation using new genetic tools that enabled the analysis of an intact organism. This allowed us to identify the origin of intercalating cells and their ability to reorient growth. Interestingly, the *ptc>rpr* lineage experiments showed respecification of the L3 vein into intervein C. As the *ara-lacZ* cells filled the whole or most of intervein C, we concluded that the gap created between L3 and L4 induced the intercalation of the missing parts that was mediated only by the anterior L3 cells. Although we cannot exclude the possibility that a few cells crossed the boundary

from the posterior to anterior in our experiments (i.e. L4 to intervein C), as previously found (Szabad et al., 1979), our present and previous observations (Bergantiños et al., 2010) demonstrated that the vast majority of cells contributing to the anterior domain had derived from anterior rather than posterior cells.

Several models have been proposed to address how the Dpp morphogen contributes to growth control and the regulation of the final size of wing discs (Schwank and Basler, 2010). We cannot discard the fact that low levels of Dpp/Hh could be acting on regenerating discs, but even if that was the case, the orientation of growth would follow different instructions from those in early disc development. Smith-Bolton et al. (Smith-Bolton et al., 2009) showed that after genetic ablation of the whole central portion of the wing pouch, regeneration and respecification proceeded before the recovery of morphogen gradients. Cell-to-cell contacts or short-range signals could stimulate and orient proliferation toward the damaged zone. We found larger clones in the central region of the disc, suggesting higher and localized growth activity instead of equally spread throughout the disc. These observations are difficult to reconcile with the concept of whole disc remodeling and recovery of morphogen scalars and thresholds. Instead, one possible explanation could be the existence of complementary factors involved in this localized proliferation, such as mechanical stretching and cell-to-cell contacts (Aegerter-Wilmsen et al., 2007; Hufnagel et al., 2007). It is possible that during the early phases of healing, cells stretch to maintain epithelial integrity and that this mechanical tension stimulates cell proliferation (Aegerter-Wilmsen et al., 2007; Shraiman, 2005).

The final size and shape of an organ depends on the coordination between cell proliferation and the spatial distribution of cells (González-Gaitán et al., 1994). This distribution can be promoted by oriented cell division. Not only in flies, but also in vertebrate development, the final shape of the limbs does not only depend on proliferation, but also on controlled orientation of cell division (Gros et al., 2010). How this orientation is achieved remains largely unknown, but the mechanism driving mitotic spindle orientation must involve interactions between cell surface and cytoskeletal proteins. For example, planar polarization of the epithelia is required for tissue shape and size determination (Lecuit and Le Goff, 2007). The protocadherin Ds that binds heterophilically to Ft is required in the wing disc for clone orientation and final organ shape (Baena-López and García-Bellido, 2003). *Ft* loss-of-function alleles generate mutants that do not reach adulthood, with the wings of the pupae or pharates being round (Garoia et al., 2005; Mao et al., 2011) and the absence of mitosis orientation along the PD axis (García-Bellido, 2009; Li et al., 2009). Thus, the planar polarity module is a good candidate for sensing external cues to drive mitotic orientation in response to an insult. *Ft* is also involved in mitotic orientation in cell competition, where fast-dividing cells orient mitosis toward the apototic cells to repopulate the tissue (Li et al., 2009). We showed here that *ft*/+ heterozygotes failed to orient their mitoses toward the death domain, generating an elongated wing. Thus, we propose that wild-type levels of *ft* are required for mitosis orientation as well as for sensing the missing domain to trigger intercalary growth.

Crb has been identified as a tumor suppressor and an upstream transmembrane component of the Hippo signaling pathway (Chen et al., 2010; Ling et al., 2010; Robinson et al., 2010). Thus, Crb is a firm candidate to transduce external cues into the nucleus. Crb, through its intracellular FERM-binding motif, directly binds to Ex (Ling et al., 2010), a cytoplasmic component that activates Hippo kinases for Yki phosphorylation, consequently preventing proliferation. Ft has also been proposed to be a potential upstream receptor in the Hippo pathway through its regulation of Ex (Bennett and Harvey, 2006; Silva et al., 2006; Willecke et al., 2006) or of the kinase Warts via Dachs (Cho et al., 2006). Moreover, after genetic ablation, Yki has been observed to enter the nucleus in the zones involved in regeneration (Grusche et al., 2011; Sun and Irvine, 2011). The dual roles of both Ft and Crb as cell-to-cell contact proteins and upstream regulators of the Hippo pathway may explain the larger and elongated wings observed in the heterozygous backgrounds. The lower availability of Ft or Crb could induce a mislocalization of Ex, facilitating the release of unphosphorylated activated Yki into the nucleus, and leading to misoriented and increased proliferation.

The possibility that increased nuclear Yki levels alter orientation was tested by overexpressing the yki^{S168A} allele, which indeed hampered orientation. Interestingly, both *crb*/+ and *ft*/+ backgrounds could be rescued and oriented properly when the *yki* dose was reduced. We cannot discard the possibility that Yki targets cell orientation, although evidence is still lacking. However, it is possible that epithelia need to balance cell proliferation and cell orientation. In conditions where there is an excess of activated *yki*, proliferation will prevail over orientation, leading to the disruption of normal organ size and shape. Thus, a balance between proliferation and the upstream cell-to-cell contact proteins that transduce external cues, such as *crb* and *ft*, must be maintained to allow mitotic orientation and the development of normal size and shape. We propose a mechanism in which cell-to-cell contacts act as sensors to coordinate cell proliferation and orientation of cell division to elicit normal organ shape and size. Thus, *crb* and *ft* are not only important for oriented growth, but also for size control. The loss of both tissue and cell-to-cell contacts could lead to overgrowth. In the cases of low *crb* and *ft* levels, the growth-promoting effect of cell ablation will result in an excess of regenerated tissue. Thus, we conclude that the recovery of normal *crb* and *ft* levels is crucial not only for oriented regenerative growth, but also for controlling the size of the regenerated tissue.

Acknowledgements
We thank A. García-Bellido, M. Milán, A. Baonza, J. F. de Celis, J. Casanova and M. Milán for fly stocks and discussions. We are particularly grateful to M. Corominas for suggestions.

Funding
C.B. was a recipient of a fellowship from the Ministerio de Educación y Ciencia of Spain. This work was supported by grants [BFU2009-09781 and CSD2007-00008] from Consolider Ingenio to F.S.

Competing interests statement
The authors declare no competing financial interests.

Author contributions
C.B. designed and conducted all experiments presented in Figs 1-4. A.R. designed and conducted all experiments presented in Figs 5 and 6. C.B., A.R. and F.S. contributed to the interpretation of the experiments. F.S. contributed to and supervised all experiments, wrote, edited and submitted the manuscript.

Supplementary material
Supplementary material available online at
http://dev.biologists.org/lookup/suppl/doi:10.1242/dev.095760/-/DC1

References

Aegerter-Wilmsen, T., Aegerter, C. M., Hafen, E. and Basler, K. (2007). Model for the regulation of size in the wing imaginal disc of Drosophila. *Mech. Dev.* **124**, 318-326.
Agata, K., Tanaka, T., Kobayashi, C., Kato, K. and Saitoh, Y. (2003). Intercalary regeneration in planarians. *Dev. Dyn.* **226**, 308-316.

Ashburner, M., Golic, K. and Hawley, R. (2005). *Drosophila: A Laboratory Handbook*. New York, NY: Cold Spring Harbor Laboratory Press.
Bachmann, A., Schneider, M., Theilenberg, E., Grawe, F. and Knust, E. (2001). Drosophila Stardust is a partner of Crumbs in the control of epithelial cell polarity. *Nature* **414**, 638-643.
Baena-López, L. A. and García-Bellido, A. (2003). Genetic requirements of vestigial in the regulation of Drosophila wing development. *Development* **130**, 197-208.
Baena-López, L. A., Baonza, A. and García-Bellido, A. (2005). The orientation of cell divisions determines the shape of Drosophila organs. *Curr. Biol.* **15**, 1640-1644.
Barrio, R. and de Celis, J. F. (2004). Regulation of spalt expression in the Drosophila wing blade in response to the Decapentaplegic signaling pathway. *Proc. Natl. Acad. Sci. USA* **101**, 6021-6026.
Basler, K. and Struhl, G. (1994). Compartment boundaries and the control of Drosophila limb pattern by hedgehog protein. *Nature* **368**, 208-214.
Bennett, F. C. and Harvey, K. F. (2006). Fat cadherin modulates organ size in Drosophila via the Salvador/Warts/Hippo signaling pathway. *Curr. Biol.* **16**, 2101-2110.
Bergantiños, C., Corominas, M. and Serras, F. (2010). Cell death-induced regeneration in wing imaginal discs requires JNK signalling. *Development* **137**, 1169-1179.
Blair, S. S. (2007). Wing vein patterning in Drosophila and the analysis of intercellular signaling. *Annu. Rev. Cell Dev. Biol.* **23**, 293-319.
Bohn, H. (1970). Interkalare Regeneration und segmentale Gradienten bei den Extremitäten von Leucophaea-Larven (Blattaria). II. Coxa and Tarsus. *Dev. Biol.* **23**, 355-379.
Bryant, P. J. (1971). Regeneration and duplication following operations in situ on the imaginal discs of Drosophila melanogaster. *Dev. Biol.* **26**, 637-651.
Bryant, S. V. and Iten, L. E. (1977). Intercalary and supernumerary regeneration in regenerating the mature limbs of Notophthalmus viridescens. *J. Exp. Zool.* **202**, 1-16.
Bryant, P. J., Huettner, B., Held, L. I., Jr, Ryerse, J. and Szidonya, J. (1988). Mutations at the fat locus interfere with cell proliferation control and epithelial morphogenesis in Drosophila. *Dev. Biol.* **129**, 541-554.
Capdevila, J., Estrada, M. P., Sánchez-Herrero, E. and Guerrero, I. (1994). The Drosophila segment polarity gene patched interacts with decapentaplegic in wing development. *EMBO J.* **13**, 71-82.
Casali, A. (2010). Self-induced patched receptor down-regulation modulates cell sensitivity to the hedgehog morphogen gradient. *Sci. Signal.* **3**, ra63.
Chen, C. L., Gajewski, K. M., Hamaratoglu, F., Bossuyt, W., Sansores-Garcia, L., Tao, C. and Halder, G. (2010). The apical-basal cell polarity determinant Crumbs regulates Hippo signaling in Drosophila. *Proc. Natl. Acad. Sci. USA* **107**, 15810-15815.
Cho, E., Feng, Y., Rauskolb, C., Maitra, S., Fehon, R. and Irvine, K. D. (2006). Delineation of a Fat tumor suppressor pathway. *Nat. Genet.* **38**, 1142-1150.
de Celis, J. F. and Barrio, R. (2000). Function of the spalt/spalt-related gene complex in positioning the veins in the Drosophila wing. *Mech. Dev.* **91**, 31-41.
Díaz-Benjumea, F. J. and García-Bellido, A. (1990). Genetic Analysis of the Wing Vein Pattern of Drosophila. *Rouxs Arch. Dev. Biol.* **198**, 336-354.
Dong, J., Feldmann, G., Huang, J., Wu, S., Zhang, N., Comerford, S. A., Gayyed, M. F., Anders, R. A., Maitra, A. and Pan, D. (2007). Elucidation of a universal size-control mechanism in Drosophila and mammals. *Cell* **130**, 1120-1133.
French, V. (1976). Leg regeneration in the cockroach, Blatella germanica. II. Regeneration from a non-congruent tibial graft/host junction. *J. Embryol. Exp. Morphol.* **35**, 267-301.
García-Bellido, A. (2009). The cellular and genetic bases of organ size and shape in Drosophila. *Int. J. Dev. Biol.* **53**, 1291-1303.
García-Bellido, A. C. and García-Bellido, A. (1998). Cell proliferation in the attainment of constant sizes and shapes: the Entelechia model. *Int. J. Dev. Biol.* **42**, 353-362.
García-Bellido, A. and Merriam, J. R. (1971). Parameters of the wing imaginal disc development of Drosophila melanogaster. *Dev. Biol.* **24**, 61-87.
Garoia, F., Grifoni, D., Trotta, V., Guerra, D., Pezzoli, M. C. and Cavicchi, S. (2005). The tumor suppressor gene fat modulates the EGFR-mediated proliferation control in the imaginal tissues of Drosophila melanogaster. *Mech. Dev.* **122**, 175-187.
Gómez-Skarmeta, J. L., Diez del Corral, R., de la Calle-Mustienes, E., Ferré-Marcó, D. and Modolell, J. (1996). Araucan and caupolican, two members of the novel iroquois complex, encode homeoproteins that control proneural and vein-forming genes. *Cell* **85**, 95-105.
González-Gaitán, M., Capdevila, M. P. and García-Bellido, A. (1994). Cell proliferation patterns in the wing imaginal disc of Drosophila. *Mech. Dev.* **46**, 183-200.
Gros, J., Hu, J. K., Vinegoni, C., Feruglio, P. F., Weissleder, R. and Tabin, C. J. (2010). WNT5A/JNK and FGF/MAPK pathways regulate the cellular events shaping the vertebrate limb bud. *Curr. Biol.* **20**, 1993-2002.
Grusche, F. A., Degoutin, J. L., Richardson, H. E. and Harvey, K. F. (2011). The Salvador/Warts/Hippo pathway controls regenerative tissue growth in Drosophila melanogaster. *Dev. Biol.* **350**, 255-266.
Grzeschik, N. A., Parsons, L. M., Allott, M. L., Harvey, K. F. and Richardson, H. E. (2010). Lgl, aPKC, and Crumbs regulate the Salvador/Warts/Hippo pathway through two distinct mechanisms. *Curr. Biol.* **20**, 573-581.
Hadorn, E. and Buck, D. (1962). Ober entwicklungsleistungen transplantierter Teilstiicke von Flugel-Imaginalscheiben von Drosophila melanogaster. *Rev. Suisse Zool.* **69**, 302-310.
Haerry, T. E., Khalsa, O., O'Connor, M. B. and Wharton, K. A. (1998). Synergistic signaling by two BMP ligands through the SAX and TKV receptors controls wing growth and patterning in Drosophila. *Development* **125**, 3977-3987.
Haynie, J. L. and Bryant, P. J. (1976). Intercalary regeneration in imaginal wing disk of Drosophila melanogaster. *Nature* **259**, 659-662.
Hinz, U., Giebel, B. and Campos-Ortega, J. A. (1994). The basic-helix-loop-helix domain of Drosophila lethal of scute protein is sufficient for proneural function and activates neurogenic genes. *Cell* **76**, 77-87.
Hufnagel, L., Teleman, A. A., Rouault, H., Cohen, S. M. and Shraiman, B. I. (2007). On the mechanism of wing size determination in fly development. *Proc. Natl. Acad. Sci. USA* **104**, 3835-3840.
Iten, L. E. and Bryant, S. V. (1976). Regeneration from different levels along the tail of the newt, Notophthalmus viridescens. *J. Exp. Zool.* **196**, 293-306.
Izaddoost, S., Nam, S. C., Bhat, M. A., Bellen, H. J. and Choi, K. W. (2002). Drosophila Crumbs is a positional cue in photoreceptor adherens junctions and rhabdomeres. *Nature* **416**, 178-183.
Karlsson, J. and Smith, R. J. (1981). Regeneration from duplicating fragments of the Drosophila wing disc. *J. Embryol. Exp. Morphol.* **66**, 117-126.
Kirby, B. S., Bryant, P. J. and Schneiderman, H. A. (1982). Regeneration following duplication of imaginal wing disc fragments of Drosophila melanogaster. *Dev. Biol.* **90**, 259-271.
Lecuit, T. and Cohen, S. M. (1997). Proximal-distal axis formation in the Drosophila leg. *Nature* **388**, 139-145.
Lecuit, T. and Le Goff, L. (2007). Orchestrating size and shape during morphogenesis. *Nature* **450**, 189-192.
Li, W., Kale, A. and Baker, N. E. (2009). Oriented cell division as a response to cell death and cell competition. *Curr. Biol.* **19**, 1821-1826.
Ling, C., Zheng, Y., Yin, F., Yu, J., Huang, J., Hong, Y., Wu, S. and Pan, D. (2010). The apical transmembrane protein Crumbs functions as a tumor suppressor that regulates Hippo signaling by binding to Expanded. *Proc. Natl. Acad. Sci. USA* **107**, 10532-10537.
Lunde, K., Biehs, B., Nauber, U. and Bier, E. (1998). The knirps and knirps-related genes organize development of the second wing vein in Drosophila. *Development* **125**, 4145-4154.
Mahoney, P. A., Weber, U., Onofrechuk, P., Biessmann, H., Bryant, P. J. and Goodman, C. S. (1991). The fat tumor suppressor gene in Drosophila encodes a novel member of the cadherin gene superfamily. *Cell* **67**, 853-868.
Mao, Y., Tournier, A. L., Bates, P. A., Gale, J. E., Tapon, N. and Thompson, B. J. (2011). Planar polarization of the atypical myosin Dachs orients cell divisions in Drosophila. *Genes Dev.* **25**, 131-136.
McClure, K. D. and Schubiger, G. (2007). Transdetermination: Drosophila imaginal disc cells exhibit stem cell-like potency. *Int. J. Biochem. Cell Biol.* **39**, 1105-1118.
Médina, E., Williams, J., Klipfell, E., Zarnescu, D., Thomas, G. and Le Bivic, A. (2002). Crumbs interacts with moesin and beta(Heavy)-spectrin in the apical membrane skeleton of Drosophila. *J. Cell Biol.* **158**, 941-951.
Mesquita, D., Dekanty, A. and Milán, M. (2010). A dp53-dependent mechanism involved in coordinating tissue growth in Drosophila. *PLoS Biol.* **8**, e1000566.
Milán, M., Campuzano, S. and García-Bellido, A. (1996a). Cell cycling and patterned cell proliferation in the Drosophila wing during metamorphosis. *Proc. Natl. Acad. Sci. USA* **93**, 11687-11692.
Milán, M., Campuzano, S. and García-Bellido, A. (1996b). Cell cycling and patterned cell proliferation in the wing primordium of Drosophila. *Proc. Natl. Acad. Sci. USA* **93**, 640-645.
Montagne, J., Groppe, J., Guillemin, K., Krasnow, M. A., Gehring, W. J. and Affolter, M. (1996). The Drosophila serum response factor gene is required for the formation of intervein tissue of the wing and is allelic to blistered. *Development* **122**, 2589-2597.
Nakamura, T., Mito, T., Tanaka, Y., Bando, T., Ohuchi, H. and Noji, S. (2007). Involvement of canonical Wnt/Wingless signaling in the determination of the positional values within the leg segment of the cricket Gryllus bimaculatus. *Dev. Growth Differ.* **49**, 79-88.
Resino, J., Salama-Cohen, P. and García-Bellido, A. (2002). Determining the role of patterned cell proliferation in the shape and size of the Drosophila wing. *Proc. Natl. Acad. Sci. USA* **99**, 7502-7507.
Robinson, B. S., Huang, J., Hong, Y. and Moberg, K. H. (2010). Crumbs regulates Salvador/Warts/Hippo signaling in Drosophila via the FERM-domain protein Expanded. *Curr. Biol.* **20**, 582-590.

Saló, E. and Baguñà, J. (1985). Proximal and distal transformation during intercalary regeneration in the Planarian Dugesia (S) Mediterranea. *Rouxs Arch. Dev. Biol.* **194**, 364-368.
Satoh, A., Cummings, G. M., Bryant, S. V. and Gardiner, D. M. (2010). Regulation of proximal-distal intercalation during limb regeneration in the axolotl (Ambystoma mexicanum). *Dev. Growth Differ.* **52**, 785-798.
Schubiger, G. (1971). Regeneration, duplication and transdetermination in fragments of the leg disc of Drosophila melanogaster. *Dev. Biol.* **26**, 277-295.
Schubiger, G. and Alpert, G. D. (1975). Regeneration and duplication in a temperature sensitive homeotic mutant of Drosophila melanogaster. *Dev. Biol.* **42**, 292-304.
Schwank, G. and Basler, K. (2010). Regulation of organ growth by morphogen gradients. *Cold Spring Harb. Perspect. Biol.* **2**, a001669.
Schwank, G., Tauriello, G., Yagi, R., Kranz, E., Koumoutsakos, P. and Basler, K. (2011). Antagonistic growth regulation by Dpp and Fat drives uniform cell proliferation. *Dev. Cell* **20**, 123-130.
Shraiman, B. I. (2005). Mechanical feedback as a possible regulator of tissue growth. *Proc. Natl. Acad. Sci. USA* **102**, 3318-3323.
Silva, E., Tsatskis, Y., Gardano, L., Tapon, N. and McNeill, H. (2006). The tumor-suppressor gene fat controls tissue growth upstream of expanded in the hippo signaling pathway. *Curr. Biol.* **16**, 2081-2089.
Smith-Bolton, R. K., Worley, M. I., Kanda, H. and Hariharan, I. K. (2009). Regenerative growth in Drosophila imaginal discs is regulated by Wingless and Myc. *Dev. Cell* **16**, 797-809.
Stocum, D. L. (1975). Regulation after proximal or distal transposition of limb regeneration blastemas and determination of the proximal boundary of the regenerate. *Dev. Biol.* **45**, 112-136.
Sun, G. and Irvine, K. D. (2011). Regulation of Hippo signaling by Jun kinase signaling during compensatory cell proliferation and regeneration, and in neoplastic tumors. *Dev. Biol.* **350**, 139-151.
Szabad, J., Simpson, P. and Nöthiger, R. (1979). Regeneration and compartments in Drosophila. *J. Embryol. Exp. Morphol.* **49**, 229-241.
Tabata, T. and Kornberg, T. B. (1994). Hedgehog is a signaling protein with a key role in patterning Drosophila imaginal discs. *Cell* **76**, 89-102.
Tabata, T., Eaton, S. and Kornberg, T. B. (1992). The Drosophila hedgehog gene is expressed specifically in posterior compartment cells and is a target of engrailed regulation. *Genes Dev.* **6** 12B, 2635-2645.
Tanaka, E. M. and Reddien, P. W. (2011). The cellular basis for animal regeneration. *Dev. Cell* **21**, 172-185.
Tepass, U., Theres, C. and Knust, E. (1990). crumbs encodes an EGF-like protein expressed on apical membranes of Drosophila epithelial cells and required for organization of epithelia. *Cell* **61**, 787-799.
Tyler, D. M. and Baker, N. E. (2007). Expanded and fat regulate growth and differentiation in the Drosophila eye through multiple signaling pathways. *Dev. Biol.* **305**, 187-201.
Willecke, M., Hamaratoglu, F., Kango-Singh, M., Udan, R., Chen, C. L., Tao, C., Zhang, X. and Halder, G. (2006). The fat cadherin acts through the hippo tumor-suppressor pathway to regulate tissue size. *Curr. Biol.* **16**, 2090-2100.
Zeidler, M. P., Tan, C., Bellaiche, Y., Cherry, S., Häder, S., Gayko, U. and Perrimon, N. (2004). Temperature-sensitive control of protein activity by conditionally splicing inteins. *Nat. Biotechnol.* **22**, 871-876.
Zhou, L., Schnitzler, A., Agapite, J., Schwartz, L. M., Steller, H. and Nambu, J. R. (1997). Cooperative functions of the reaper and head involution defective genes in the programmed cell death of Drosophila central nervous system midline cells. *Proc. Natl. Acad. Sci. USA* **94**, 5131-5136.